Development of biocompatible plasmonic thin films composed of noble metal nanoparticles embedded in a dielectric matrix to enhance Raman signals

Diogo Costa[1,2], João Oliveira [1], Marco S. Rodrigues[1], Joel Borges[1*], Cacilda Moura[1], Paula Sampaio[2], Filipe Vaz[1**]

[1]Centro de Física, Universidade do Minho, Campus de Gualtar, 4710 - 057 Braga, Portugal
[2]Centro de Biologia Molecular e Ambiental (CBMA), Universidade do Minho, Campus de Gualtar, 4710 - 057 Braga, Portugal

Corresponding authors:
*Joel Borges; e-mail: joelborges@fisica.uminho.pt
**Filipe Vaz; e-mail: fvaz@fisica.uminho.pt

Abstract

This work focused on the production of nanocomposite thin films, composed of noble nanoparticles embedded in a dielectric matrix, to be tested as biocompatible plasmonic platforms for detection of molecules using Surface Enhance Raman Spectroscopy (SERS). Three different thin films systems were deposited by reactive DC magnetron sputtering, namely Au-Al_2O_3, Au-TiO_2 and Ag-TiO_2. The depositions were followed by a thermal treatment at different temperatures to promote the growth of the nanoparticles. Localized Surface Plasmon Resonance (LSPR) bands appeared already at 300 ºC, related to the presence of Au nanoparticles, and at 500 ºC in the case of Ag nanoparticles. Furthermore, at 700º C, the Ag-TiO_2 films showed a broadband optical response due to the formation of Ag clusters at the film's surface. The biological experiments showed that the presence of the thin films didn't affect the growth of *C. albicans*, which is very convenient if one needs to detect low concentrations of this microorganism using SERS platforms. As for the SERS

measurements, an enhancement of R6G Raman spectra intensity was clearly perceivable, but only for the TiO_2 matrix. Furthermore, the application of a plasma treatment allowed to better expose the nanoparticles, providing a further enhancement of Raman signals.

Keywords:

Thin films; Nanoparticles; Oxide matrix; Localized Surface Plasmon Resonance; *C. albicans*; Surface Enhanced Raman Spectroscopy.

Highlights:

- Plasmonic thin films of Au-Al_2O_3, Au-TiO_2 and Ag-TiO_2 were prepared;
- Annealing treatments affect the microstructure and plasmonic response;
- Cellular growth of *C. albicans* in not affect by the presence of the films;
- Plasma treatments on Au-TiO_2 and Ag-TiO_2 enhances Raman signals of R6G molecules;
- A relative SERS enhancement factor of 10^2 was obtained.

1. Introduction

Nanoscale tailoring of materials allows to obtain physical and chemical properties that differ from bulk counterparts [1]. Among several examples, are the nanostructures composed of noble metals (e.g. gold and silver nanoparticles), which present nanoplasmonic properties that can be used in different applications [2,3]. In a metallic surface, collective electronic excitations in the metallic/dielectric interface, associated with an oscillating electromagnetic field, originate surface plasmons [4,5]. If these surface plasmons propagate along a continuous metallic surface, they are designated as surface plasmon polaritons (SPP) [6,7]. When confined to a metallic nanostructure or nanoparticle are mentioned as localized surface plasmons (LSP) [8]. In this regard, Localized Surface Plasmon Resonance (LSPR) became a subject of great interest in research due to the multitude of applications that arise from this phenomenon [9,10]. Aside from decorative purposes, many technological applications of LSPR can be found in the literature, such as plasmonic sensors for gas and biomolecular detection, plasmon based photo-detectors, phototherapies and surface enhanced Raman spectroscopy (SERS) [11,12].

LSPR is characterized by strong electromagnetic field enhancements near the nanostructure and strong extinction (absorption + scattering) bands, and these properties can be tuned by changing some nanostructural characteristics [13,14]. Some of them are the geometry, size, shape and distribution of the nanoparticles embedded in a dielectric medium, which are known to affect the LSPR absorption band [15–18]. Furthermore, the atomic number and concentration of metal composing the nanoparticles also affect the LSPR properties, as well as the dielectric function of the surrounding medium [9,15]. Tailoring these parameters allows to obtain plasmonic nanostructures with absorption bands in the visible range of the electromagnetic spectrum, revealing a great potential to the construction of optical biosensors.

It is well-known that Surface Plasmon Resonance (SPR) sensors have high sensitivities, due to the long decay length of its evanescent field, and are already widely applied in biosensing [19]. On the

other hand, LSPR presents highly confined and intense electromagnetic fields around the nanostructure. This leads to a lower sensing volume, comparing to SPR sensing, but, consequently, the analyte occupies a much larger portion of the sensing area [13,20]. Another benefit of LSPR is that it can be excited by passing-through light (transmittance mode T-LSPR) [21], and this allows the use of ordinary optical equipment to observe the T-LSPR band and monitor its evolution in the presence of different analytes [22].

Furthermore, using LSPR in biosensing isn't limited to optical sensors. Applying LSPs to Raman spectroscopy allows the enhancement of commonly low signal intensity, resulting in Surface-Enhanced Raman Spectroscopy (SERS) [23,24]. Raman spectroscopy relies on the phenomenon of inelastic scattering, defined by the energy difference between incident photons and vibrational modes [25–27]. As consequence, each (bio)molecule will have a unique Raman spectrum, acting as a fingerprint for that molecule [28]. In this respect, the high intensity and confinement of electromagnetic fields near the nanoparticles in LSPR, can benefit Raman spectroscopy, by enhancing the Raman signal intensity of a molecule placed in the sensing area of a nanoparticle [29]. This electromagnetic enhancement enables the detection of very low concentrations of molecules as it can reach enhancement factors up to 10^{14} [30–32].

One of the possible use of SERS technology is the quick detection and identification of individual cell types, from microorganisms to cancer tissue and stem cells [33–35]. The produced molecular fingerprints by Raman spectroscopy can be used to identify and differentiate compounds, and can possibly be used to create a signature database for Raman spectroscopy identification [36]. As the spectra are reproducible, they are highly adequate for identification of fungi [37,38]. More specifically, in the case of microorganisms, the rapid identification of significant species is of utmost importance to choose the appropriate therapy, which can be related to the morbidity and mortality rates [39]. The identification of *Candida spp.* by Raman spectroscopy is already described in the literature [40,41].

In terms of nanoplasmonic transducers, most research is done in nanoparticles produced by chemical methods or nanolithography in the production of LSPR platforms [42]. However, these techniques reveal problems like high production cost or environmental problems [9,43]. In this field, some research has been done in magnetron sputtered thin films consisting of noble metal nanoparticles embedded in a dielectric matrix [44,45]. Changing the deposition parameters of these films, as well as the post-deposition thermal treatment conditions, allows to tune LSPR bands within the visible spectra by changing some nanostructural parameters (size, shape and distribution of the nanoparticles), the noble metal concentration, and also the dielectric matrix (usually an oxide) [46–49]. However, to achieve high Raman signal enhancements, it is necessary to ensure that a high number of nanoparticle "hotspots" are found in the surface. It was shown by Rodrigues *et al.* that using plasma etching it is possible to promote the erosion of the matrix surface, allowing for the exposure of more metallic nanoparticles [50].

In this work, different series of plasmonic thin films were prepared, in order to study the influence of plasmonic metal (Au or Ag) and dielectric matrix (TiO_2 and Al_2O_3) on the main characteristics and properties of the films. They consist of Au-TiO_2, Ag-TiO_2 and Au-Al_2O_3 deposited by reactive magnetron sputtering. To induce the growth of the nanoparticles and thus to obtain LSPR bands, observable in the transmittance spectrum, the films were submitted to post-deposition thermal annealing. In terms of applications, the thin films were evaluated as SERS platforms using R6G as well as in cellular cultures of *Candida albicans* to explore the possibility of using the plasmonic thin films as SERS chips to detect microorganisms.

2. Experimental details

2.1 Preparation and microstructural characterization of the nanoplasmonic thin films

The thin films were prepared by reactive DC magnetron sputtering and deposited in glass lamellae, fused silica and Si (p-type, Boron doped) substrates. For TiO_2 matrix thin films, the cathode was a titanium target (99.99 % purity) with rectangular dimensions, 200×100×6 mm^3, on which gold or silver pellets were placed in the preferential erosion zone of the target, as the objective was to produce Au-TiO_2 and Ag-TiO_2 thin films, with a total area of 32 mm^2. A current of 2 A was applied (current density of 100 $A.m^{-2}$), and the generated plasma was composed by argon (partial pressure of 3.3×10^{-1} Pa) and O_2 (partial pressure of 7.8×10^{-2} Pa). For Al_2O_3 matrix, the cathode was an aluminum target (99.99% purity), also with a total area of Au pellets of 32 mm^2 incrusted in its preferential erosion track. A current of 1.5 A was applied (current density of 75 $A.m^{-2}$) in a plasma composed by argon (partial pressure of 4.1×10^{-1} Pa) and O_2 (partial pressure of 9.2×10^{-2} Pa). The substrates were placed in a grounded sample holder, rotating at 5 rpm.

To promote the growth of the nanoparticles in the matrix, the thin films were subjected to post-deposition annealing treatments, with heating ramps of 5 ˚C/min and different isothermal temperatures (300, 500 and 700 ˚C), followed by a free cool down to room temperature.

The in-depth chemical composition profile was evaluated by Rutherford Backscattering Spectrometry (RBS). The measurements were performed with a 2 MeV $^4He^+$ ion beam at an incidence angle of 0°. The detection system was composed by three detectors: a standard at 140º and two pin-diode detectors located symmetrical to each other, both at 165º (with detector 3 on the same side as the standard detector 2). The collected data were analyzed with IBA DataFurnace NDF v9.6a [51–53]. Morphological features were analyzed by Scanning Electron Microscopy (SEM), in a Dual Beam SEM/FIB FEI Helios 600i microscope. The thickness was also measured through the observation of the cross-sections of the as-deposited thin films.

The crystalline structure of the films was obtained by *in situ* high temperature X-ray diffraction (HT-XRD), in a Bragg–Brentano configuration using the Brucker D8 diffractometer equipped with Cu-Kα radiation (λ = 0.154 nm). The measurements were conducted using the same conditions as the annealing step. Furthermore, the size of the Au or Ag crystalline domains was determined by fitting the preferential growth diffraction peaks with *Pearson VII* functions, using the *Winfit* software [54]. The films' surface roughness was obtained by Atomic Force Microscopy (AFM), using a MultiMode SPM microscope, controlled by a NanoScope IIIa from Digital Instruments, in tapping configuration. Transmittance spectra, in the range of wavelengths from 300 to 900 nm, with a step of 0.5 nm, were measured using a Shimadzu UV-2450(PC) spectrophotometer.

2.2 Growth behavior of C. albicans on Au-Al_2O_3, Au-TiO_2 and Ag-TiO_2 thin films

The growth behavior was evaluated by the interaction of the yeast cells with the surface of the plasmonic thin films, annealed at different temperatures. A pre-culture of yeast cells was prepared from a cell colony and inoculated in a culture tube with 20 mL of Yeast Peptone Dextrose (YPD) medium (1% yeast extract (w/v), 1% bactopeptone (w/v), 2% Glucose (w/v)). This pre-culture was incubated overnight at 30 °C. The thin films (in Si wafer of 2.25 cm^2) were sterilized with 70% ethanol for 2 hours and then washed using sterile water. On the next day, the cells were transferred to culture tubes with 20 mL of YPD medium with the thin films, at an initial optical density (OD) of 0.1 at 600 nm of wavelength. The cells were incubated at 30 °C and shaken at 120 rpm. The OD at 600 nm in a Spectronic 20 spectrophotometer was monitored during the 25 hours of the experiment. For further evaluation of the interaction between cells and the thin films' surface, two time points were selected, one in the microbial exponential growth phase (8 hours) and another in the later stationary growth phase (25 hours). At these selected time points the number of viable cells after the interaction of the thin film was estimated by counting the colony forming units (CFUs).

CFUs data from three independent experiments were analyzed using one-way ANOVA, with Dunnett's multiple comparisons test, with 95% confidence level, using GraphPad Prism 6 software (GraphPad Software, Inc., La Jolla, CA, USA). The objective was to test if the results from the incubation of *C. albicans* with the thin films were significantly different from the control group growth over the thin films substrate (silicon wafer).

2.3 RAMAN measurements in plasmonic thin films

Plasma treatment was performed in all samples at 700 °C annealing to increase the number of nanoparticles partially exposed to the surface, as showed by Rodrigues *et al.* [50].

For surface-enhanced Raman spectroscopy measurements, a 20 µL droplet of a 2×10^{-4} M Rhodamine 6G solution in ethanol was placed on top of the samples and left to dry overnight. The SERS measurements were performed at room temperature with a Horiba Jobin Yvon T64000 triple Raman spectrometer, equipped with liquid nitrogen cooled charge coupled device (CCD) Symphony II 1024 × 246 FIVS detector, with a resolution better than 1 cm^{-1}. The excitation line, 514.5nm, of an argon ion laser, was focused onto the sample using a ×50 MS Plan objective of an Olympus Microscope BHSM, in a back-scattering geometry. The spectra were obtained with a measured power of about 0.4 mW onto the sample, during an integration time of 30 s, with 5 measurements per sample.

3. Results and discussion

3.1 Composition and microstructure of the as-deposited films

RBS analysis allowed to determine the atomic concentration of noble metal in each deposited thin film series. In the films with aluminum oxide matrix, Au-Al_2O_3, the atomic concentration of Au was 17 at.%. Regarding the TiO_2 matrix, 13 at.% of Au was found in the Au-TiO_2 films and 19 at.% of Ag for the Ag-TiO_2 films. RBS analysis showed that there was a higher gold content in the Al_2O_3 matrix, comparing to the TiO_2 matrix, for the same amount of gold in the target (two pellets). This could be due to the difference in the applied current to the sputtering target, as previously shown, a higher current causes a lower effective Au sputtered area [50], and also the lower sputtering yield of Al_2O_3 compared to TiO_2 [55]. Changing the noble metal into the TiO_2 matrix from Au to Ag displayed different noble metal concentrations in the thin films. In fact, Ag-TiO_2 thin films have a higher noble metal content, as the silver has a higher sputtering yield compared to gold [56].

As for the SEM analysis, it allowed to observe the morphology, as well as the thickness of the as-deposited thin films. The micrographs in Figure 1 show a featureless-dense morphology for the Au-Al_2O_3 and a thinner film. The microstructure of Au-TiO_2 thin film is also relatively dense, though more granular and thicker, while the Ag-TiO_2 thin film reveals a more porous microstructure. This behavior is not only related to the higher content of plasmonic metal dispersed in the TiO_2 matrix, but also due to the growth of more disordered microstructures associated to the presence of Ag instead of Au [57].

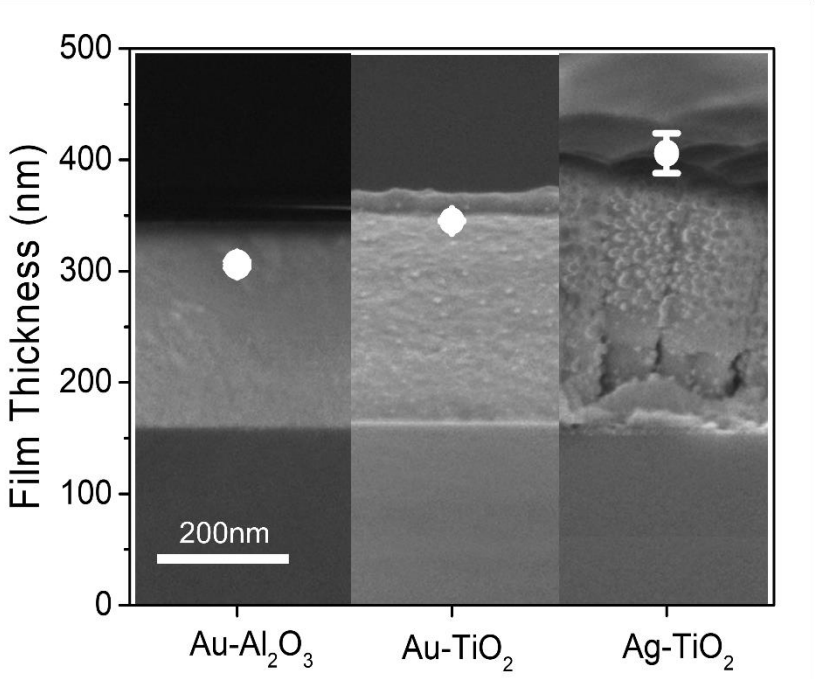

Figure 1 - Thickness measurement and SEM micrographs of as-deposited thin films: Au-Al_2O_3; Au-TiO_2 and Ag-TiO_2.

3.2 The growth of plasmonic nanoparticles via thermal annealing

3.2.1 Structural evolution of the films using in situ XRD annealing

X-Ray diffraction showed an amorphous structure for all as-deposited thin films (Figure 2). In the Au-TiO_2 thin films (Figure 2a) Au starts to crystallize in fcc structure after annealing at 300 ˚C, as evidenced by the diffraction peak (111) appearing at 38.1˚. At this temperature the TiO_2 matrix also starts to crystalize into the anatase phase, as revealed by the faint peak (101) at 25.3˚ [ICDD: 44882]. The anatase phase is characteristic of the Au-TiO_2 thin films annealed to temperatures above 300 ˚C, as shown in previous works [58,59]. At 500 ˚C, the (111) diffraction peak becomes more intense, while the (200) diffraction peak related to the crystallization of Au appears at 44.4˚. Finally, at 700 ˚C, the diffractions peaks (111) and (200) related to Au crystallization become even more intense and sharper since the crystalline domains of Au are larger. As for the matrix, the diffractograms show the crystallization of TiO_2 in its rutile phase for temperatures of 700 ˚C,

showed by the diffraction peak positioned at 27.4˚, indexed to the (110) orientation of the rutile structure [ICDD: 62677]. Furthermore, at 700 ºC both phases coexist in the film, anatase and rutile. Concerning the Ag-TiO_2 films (Figure 2b), it is possible to differentiate from the Au-TiO_2 system as the diffractograms don't show any diffraction peaks related to the crystallization of Ag or TiO_2 at 300 ˚C. Increasing the temperature to 500 ˚C led to the crystallization of Ag in the fcc structure, as a sharp diffraction peak appears for a 2Θ angle of 38.1˚ [COD-1100136] related to the (111) orientation of the fcc structure of crystalized Ag. However, contrarily to thin films of Au-TiO_2, where it is possible to observe the anatase phase at 500 ˚C, the presence of Ag in the TiO_2 matrix inhibits the formation of anatase phase [47,60]. Further increase of the annealing temperature to 700 ˚C led to the appearance of sharp and intense peaks, corresponding to the (111) and (200) orientations of Ag structure, the latter appearing at a 2Θ angle of 44.4º [COD-1100136]. Concerning the TiO_2 matrix, after annealing at 700 ˚C, the matrix crystallizes into the rutile phase, with an intense and well-defined diffraction peak at 27.4˚ [ICDD: 62677], correspondent to the (110) orientation of this phase. Therefore, when compared to Au, the Ag atoms promote the formation of rutile instead of anatase [47].

Finally, in Au-Al_2O_3 thin films (Figure 2c), and similarly to Au-TiO_2 system, it is possible to observe the crystallization of Au in the face centered cubic structure at 300 ˚C, with the appearance of the (111) diffraction peak at a 2Θ angle of 38.2˚ [ICDD: 04-0784]. At 500 ˚C, the (111) diffraction peak increases in intensity, and the diffraction peak related to the (200) orientation of the fcc structure of Au appears at 44.4˚ [ICDD: 04-0784]. After annealing at 700 ˚C, both diffraction peaks increase in intensity and become slightly narrower. However, the annealing process didn't induce any crystallization of the Al_2O_3 matrix.

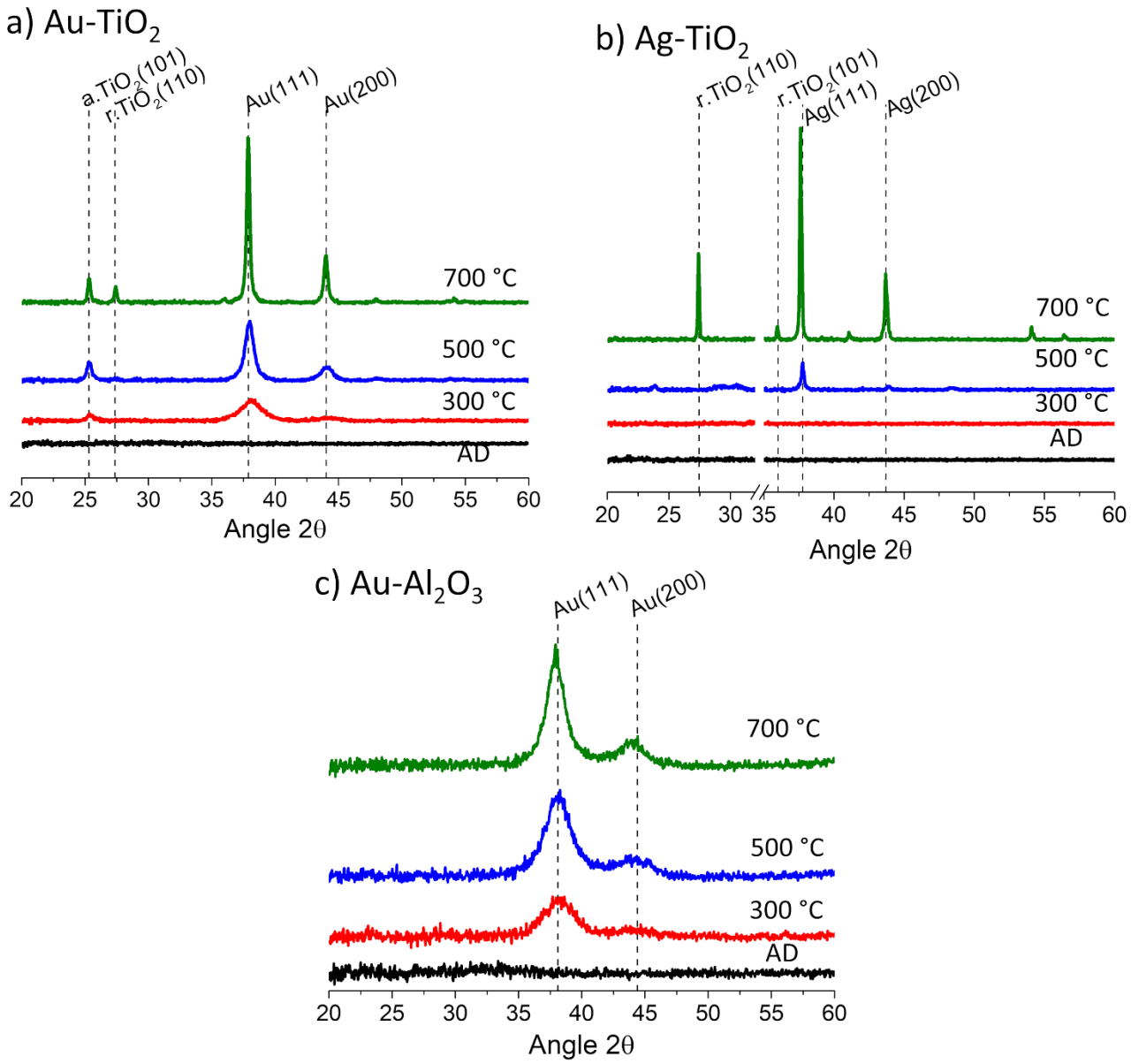

Figure 2 - XRD diffractograms of the as-deposited and annealed thin films: (a) Au-TiO_2, (b) Ag-TiO_2 and (c) Au-Al_2O_3.

Using the preferential growth orientation of the noble metals (Au or Ag), the grain sizes were estimated for the thin films annealed from 300 to 700 ˚C. The simulation consisted of fitting Pearson VII functions to the diffractograms of the thin films in the (111) diffraction peak for Au and Ag. The grain size of Au-Al_2O_3 thin films suffers a slight increment from 2 to 4 nm with the

increase of annealing temperature from 300 to 700 ˚C. For the same temperature interval, in the Au-TiO_2 system, the grain size variation is more significant, changing from 3 to 9 nm as the temperature is increased from 300 ºC to 500 ˚C, and increases even further to 33 nm, with an annealing temperature of 700 ˚C. The differences in growth of the Au nanoparticles between the Al_2O_3 and TiO_2 matrixes is most likely related to the structural evolution of the matrixes during the annealing. It has been shown that the crystallization of TiO_2 increases the number of grain boundaries [61], leading to a higher diffusion of gold trough these boundaries, where the nanoparticles can more easily aggregate and suffer coalescence and/or Ostwald ripening phenomena, resulting in the formation of larger nanoparticles. On the other hand, the lack of crystallization of the Al_2O_3 matrix prevents the formation of grain boundaries, hindering the diffusion of Au throughout the matrix thus inhibiting the growth of large crystalline domains of Au [62].

Table 1 - Mean grain size of Au and Ag crystalline domains for the different thin films annealed at different temperatures.

Annealing temperature	**Noble metal grain size (nm)**		
	Au-Al_2O_3	Au-TiO_2	Ag-TiO_2
300°C	2	3	-
500°C	3	9	61
700°C	4	33	141

Finally, since the Ag-TiO_2 thin films don’t present crystallization of the silver atoms at 300 ˚C, no value of grain size is obtainable for this annealing temperature. However, at 500 ˚C, the grain size of the crystalline domains of Ag is considerably higher than the Au systems: 61 nm. Moreover, it further increased to 141 nm when the annealing temperature was 700 ˚C. These values strongly

suggest that Ag crystals have diffused to the surface of the thin films, a typical behavior of this kind of films [47,60].

3.2.2 Surface roughness of the films

An important thin film's feature when they interact with different analytes such as cells is the surface roughness [63]. Using AFM, it was possible to measure the surface roughness of the thin films at the different annealing temperatures. As-deposited Au-Al_2O_3 films have a very smooth surface, with a root mean square (RMS) roughness of approximately 2.0 nm. The annealing treatment at 300 ºC didn't affected the roughness of the films but increasing the temperature to 500 °C promoted an increase of roughness to 4.2 nm. Nevertheless, unexpectedly the increase of the annealing temperature from 500 °C to 700 °C led to a small decrease in roughness of the films from 4.2 to 2.9 nm. This decrease in surface roughness could be due to the densification of the Al_2O_3 matrix, as already reported [55].

Considering the Au-TiO_2 thin films, the surface roughness of the thin films increases with the annealing temperature (Figure 3). From as-deposited to 300 °C, the roughness increases from 1.6 to 4.7 nm, respectively. This increase is most likely due to the beginning of the crystallization of Au and TiO_2 into anatase. From 300 °C to 500 °C, the roughness remains approximately the same, despite the crystallinity improvement. Only when the rutile phase appears, at 700 °C, it is possible to observe another increment of the film's roughness from 4.3 to 6.5 nm.

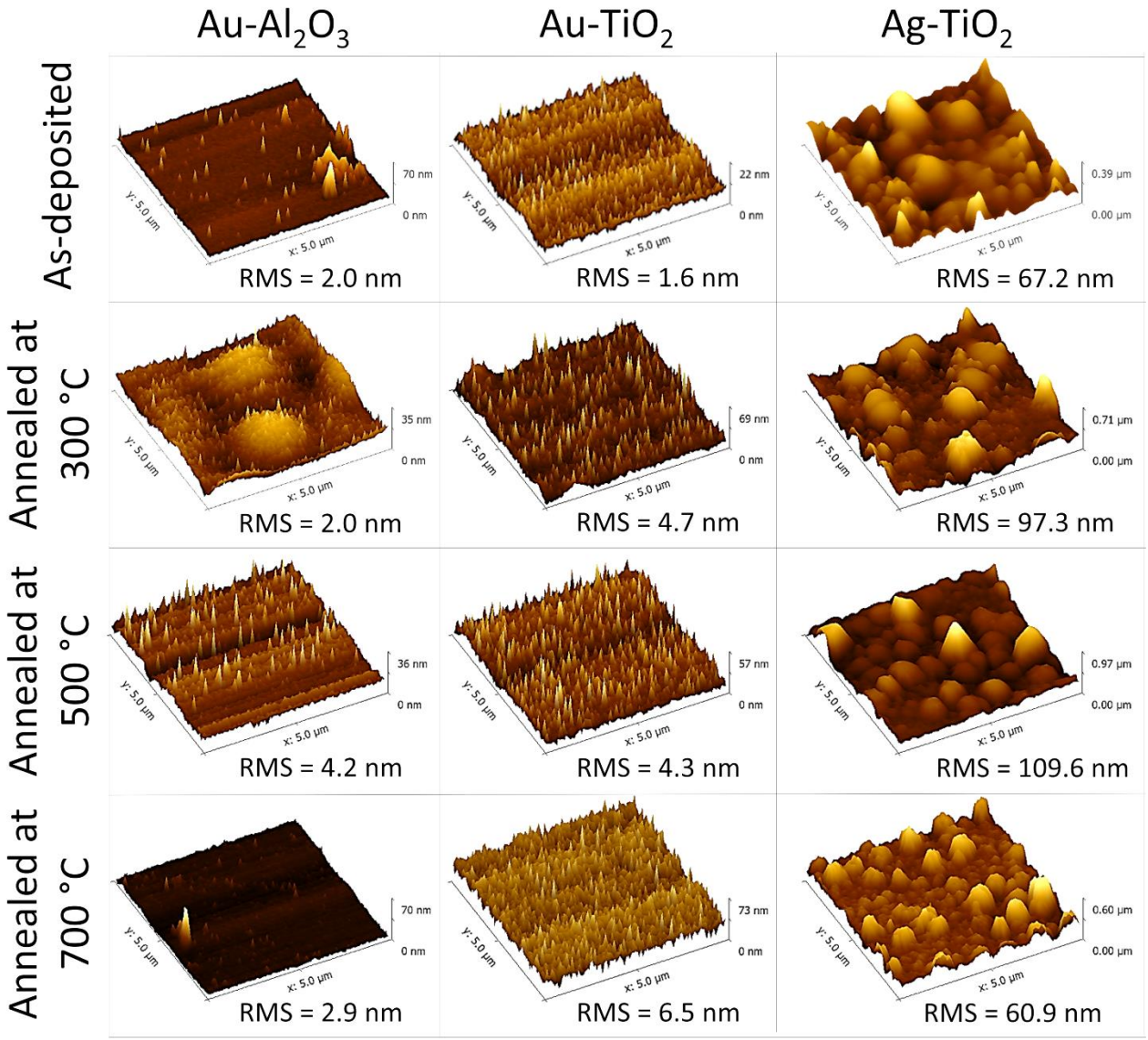

Figure 3 - Topographic images obtain by AFM for the as-deposited and annealed thin films with RMS roughness measurements.

Finally, Ag-TiO_2 thin films reveal a very different surface topography, in comparison with Au-Al_2O_3 and Au-TiO_2 thin films. The film as-deposited has a relatively much higher roughness, about 67.2 nm, as the presence of Ag seems to greatly affect the thin film microstructure. Further increasing the annealing temperature to 500 °C led to an increase of roughness to 109.6 nm. This may be due to the crystallization of Ag embedded in the TiO_2 matrix. From 500 °C to 700 °C of annealing temperature, the surface roughness decreases, from 109.6 to 60.9 nm, as the matrix crystallizes in

the rutile phase and crystallization of Ag increases in intensity. This lower surface roughness could also be due to the formation of large Ag crystals in the surface of the thin film, in contrast with the film's surface, as seen by Borges *et al.*, due to the coalescence of silver [57]. In the AFM 3D images, the presence of large structures is clear.

3.3 Optical response of the films (LSPR bands)

Regarding the Au-TiO_2 thin films (Figure 4a), interference behavior appears for the as-deposited film, with no LSPR band observable in the transmittance spectrum. Through the annealing process, it was induced the growth of Au nanoparticles that stayed embedded into the TiO_2 matrix. At 300 ºC, the transmittance drastically decreases to below 6%. A broad LSPR absorption band is observable in the wavelength range from 500 nm to 750 nm. Further increasing the thermal treatment temperature to 500 ºC induced a higher crystallization of the Au embedded in the anatase the matrix. In terms of the LSPR absorption band, the film annealed at 500 ºC showed an increase of overall transmittance and narrowing of the band itself, presenting a more defined LSPR band due to the increase of gold nanoparticles. Finally, when the annealing temperature reaches 700 ºC, the LSPR band became broadened, and the band minimum reached zero transmittance, extending from 550 nm of wavelength to 800 nm. This is in accordance with the coalescence of the gold nanoparticles into large spheroidal shaped clusters, as predicted in theoretical studies of this plasmonic system [64].

As for the Ag-TiO_2 thin films (Figure 4b), the as-deposited thin film shows a lower transparency, when compared to the gold counterpart, yet presenting an interference-like behavior. The annealing temperature of 300 °C results in an increase of transmittance but maintaining the interference behavior observed in the as-deposited film. This is due to the lack of crystallization and aggregation of Ag in nanoparticles, as the XRD results had previously shown. The transmittance spectra of the film annealed at 500 °C shows a faint LSPR band at about 565 nm. The appearance of the LSPR

effect is related to the crystallization of Ag and its aggregation into nanoparticles. Nevertheless, at 700 °C, where the crystallization of Ag presents a diffraction peak of high intensity, and the matrix also is crystallized in the rutile phase, the film has an almost constant absorption throughout almost the whole spectra. This optical response is a consequence of the diffusion of Ag towards the surface of the films, aggregating in large crystals or even fractal structures [57].

Finally, the changes induced in the transmittance spectra of Au-Al_2O_3 thin films due to thermal annealing are presented in Figure 4c. The as-deposited thin film shows an interference pattern, with no evidence of a T-LSPR band. This behavior is in agreement with the amorphous structure of the film showed by XRD, suggesting that gold is dissolved in the matrix or might be present in the form of very small clusters. Annealing the film at 300 °C induces the crystallization of Au and its aggregation in nanoparticles. At this temperature, it's possible to observe an accentuated decrease in transmittance, near 560 nm compared to the as-deposited sample, due to the appearance of a LSPR band. However, this band starts at 475 nm until 650 nm, making a wide and low intensity LSPR band. Further increasing the annealing temperature to 500 ºC and then to 700 ºC led to an increase in Au crystallinity and grain size, and these morphological changes decreased the overall transmittance spectrum and thus the LSPR band, which also became broader with the increase of the temperature.

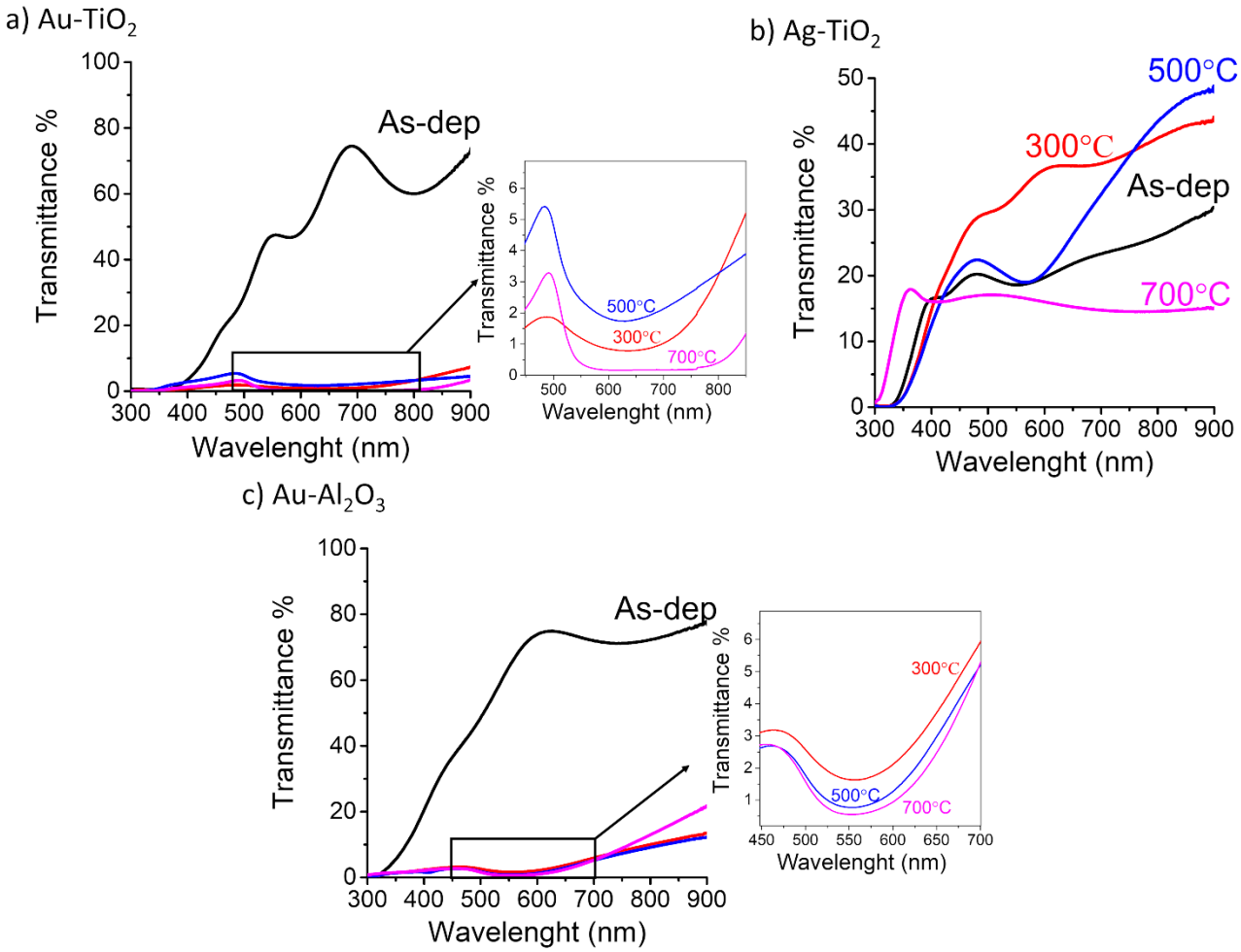

Figure 4 - Evolution of the transmittance spectra with the annealing treatment at different temperatures for the deposited thin films: (a) Au-TiO_2; (b) Ag-TiO_2 and (c) Au-Al_2O_3.

3.4 Interaction of C. albicans with plasmonic thin films

Characterizing the plasmonic thin films in terms of interfering with cell viability may provide useful information when considering the construction of a biosensor to detect live cells or monitoring the growth of a certain species.

C. albicans, a pathogenic yeast species, was incubated for 25 hours in YPD medium in the presence of Au-Al_2O_3, Au-TiO_2 and Ag-TiO_2 thin films at different annealing temperatures (as-deposited, 300, 500 and 700 °C) to evaluate cell viability, and results are presented in Figure 5.

Firstly, growth curves were plotted as optical density measurements, at 600 nm wavelength, at different timepoints for 25 hours, Figure 5a. From the growth curves, it is possible to perceive that the presence of the plasmonic thin films in the growth medium didn't affect significantly the growth of the yeast cells, when compared to the control group.

Using the exponential growth phase of the growth curve, it is possible to determine the specific growth rate of the cells in the presence of the thin films and compare it to the control group, Figure 5b. Since the analysis of the growth curve of *C. albicans* didn't show any significant differences, the specific growth rate was similar among the thin films, as expected.

Nonetheless, colony forming units were counted at two distinct time points: one in the exponential growth phase (8 hours) and another at the final growth phase (25 hours) to evaluate cells viability (Figure 5c), for each series of thin films with different annealing temperatures. Comparing the results with the control group, the thin films had no significant effect on the viability of the yeast cells, both after 8 hours and 25 hours of incubation, with no signs of cellular death or growth inhibition.

Therefore, the results show that the proposed thin films have no effect on the growth and viability of the tested microorganisms and may be used for creating biosensors for cellular entities.

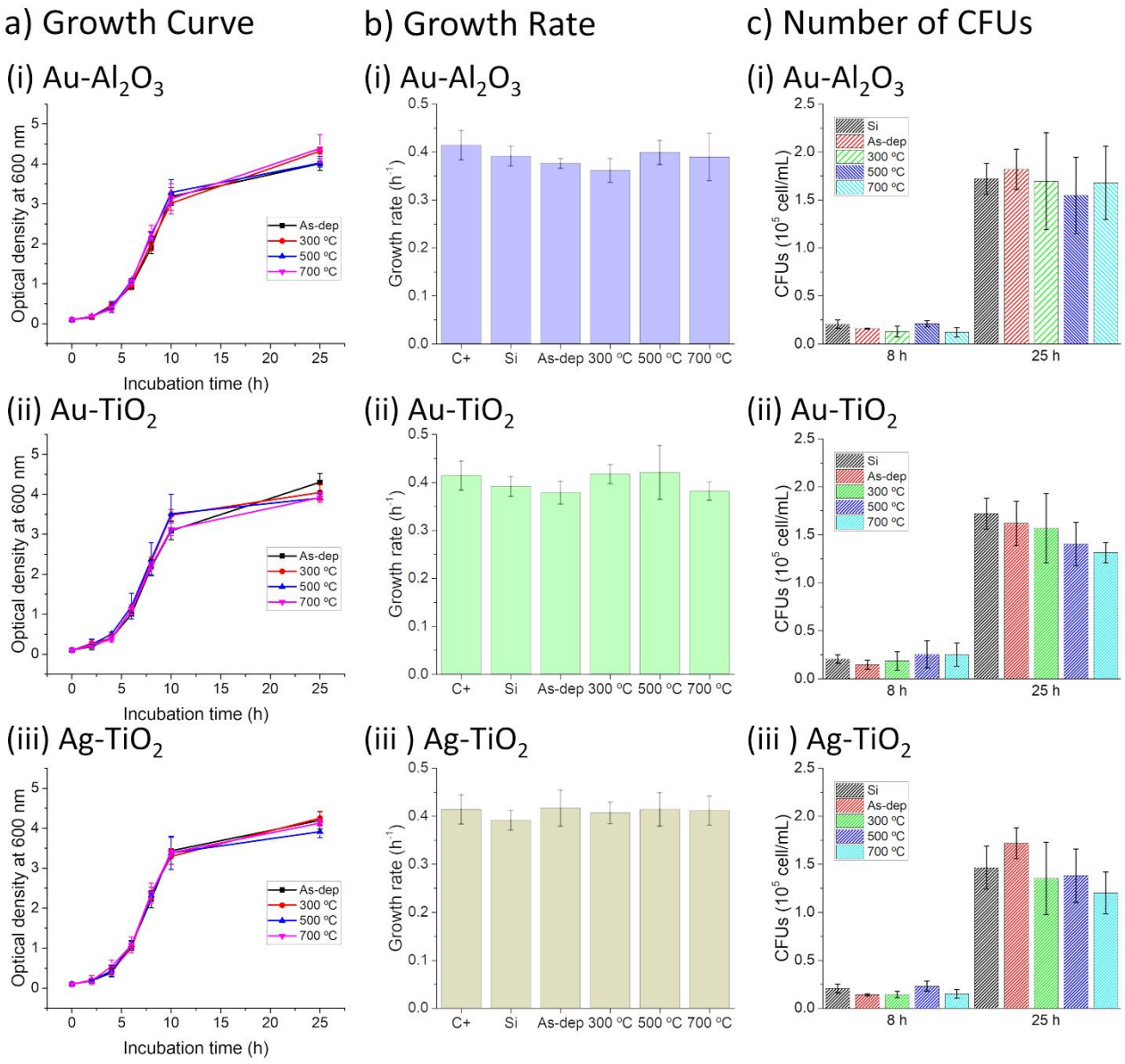

Figure 5 - Cellular growth of *Candida albicans* interacting with the thin films at different annealing temperatures: a) growth curve given at optical density at 600 nm; b) growth rate for yeast cultures in contact with the film's surface; c) number of CFUs counted for the selected time points, 8 and 25 hours of incubation (one, two, three and four * are related to the statistical significance of the results and correspond to $P < 0.05$, $P < 0.01$, $P < 0.001$ and $P < 0.0001$, respectively).

3.5 Surface enhancement of Raman spectra using the plasmonic thin films

Plasmonic thin films present interesting applications for Raman spectroscopy, as they can enhance the signal by several orders of magnitude [65]. The enhancement factor is an important metric to compare the performance between different plasmonic systems, but quantifying the enhancement isn't a trivial endeavor. The enhancement factor depends on several factors, some of them related to the material itself, but also with the studied probe and the experimental apparatus [65]. However, if the measurements are carried out in the same experimental conditions, the difference of peaks' amplitude between samples is the same as the difference of enhancement for those specific conditions. Thus, it is possible to compare the performance of the thin films, at least for this restrictive set of experimental conditions.

The SERS spectra bring a second difficulty, as it's common to observe significant non-uniform fluorescence, which makes their analysis challenging but needs to be considered to get an accurate fit. For this, Moores *et al.* developed a fitting algorithm for SERS spectra that assumes the spectrum as a series of peaks plus a smoothly varying baseline typical of fluorescence [66].

Density-functional theory (DFT) calculations can be used to predict the vibrational frequencies and assign the vibrational modes. The DFT and experimental results obtained by Watanabe *et al.* for Rhodamine 6G adsorbed on silver were used to identify peaks [67], as well as the provided R package implementation of the algorithm provided by Moores *et al.* [66] to fit the spectra. The peaks were modeled using pseudo-Voigt functions.

The experimental results and the resulting fits are displayed in Figure 6. The Au-Al_2O_3 system did not show a clearly measurable signal related to the presence of R6G molecules, even after the films being subjected to plasma treatment. The behavior of this system is surely related to the poor crystallization of Au nanoparticles throughout the Al_2O_3 matrix, in agreement with the structural analysis.

For Au-TiO_2 and Ag-TiO_2, with and without plasma treatment, it is possible to observe peaks related to the presence of R6G. Figure 6b-i shows the Raman spectrum for Au-TiO_2, without plasma treatment. When compared to the corresponding spectra of Ag-TiO_2 (Figure 6c-i), the latter have much higher intensities for the same Raman peaks (the plots are not in the same intensity scale). Therefore, the replacement of Au by Ag into a TiO_2 matrix enhances Raman signals, and the reason for this behavior is related to the higher nanoparticles' size that were obtained after the thermal treatment.

Furthermore, both plasmonic systems have shown enhancement of the R6G signals after plasma treatment. The effect of the plasma treatment is to further expose some of the embedded nanoparticles to the environment, increasing adsorption areas. This turns the thin films more sensitive to the presence of analytes, as can be confirmed by the respective Raman spectra.

From the obtained fits, the intensity of the Raman signal at 1363 cm^{-1} on the Ag-TiO_2 thin films is around one order of magnitude below the fluorescence and around the same order on Au-TiO_2. The R6G molecules have conventional Raman cross section of 10^{-30} cm^2 per molecule, however, at the excitation wavelength used of 514.5 nm, the fluorescence cross section of the R6G is on the order of 10^{-16} cm^2 per molecule [68]. So, it is possible to infer that the measured Raman signal of R6G has a cross section of around 10^{-15} cm^2 and an enhancement of 10^{15} on the Ag-TiO_2 system, while a cross section of 10^{-16} cm^2 and an enhancement of 10^{14} was estimated for the Au-TiO_2 system. However, the used wavelength is within the absorption band of the R6G, and therefore the signal enhancement comes from two sources: the substrate with metallic nanoparticles and the R6G Resonant Raman Scattering. At the used wavelength of 514.5 nm, the enhancement from Resonant Raman Scattering for R6G molecules is in the order of 10^4 [69]. Subtracting the resonant enhancement leaves the contribution of 10^{11} for Ag-TiO_2 and 10^{10} for Au-TiO_2.

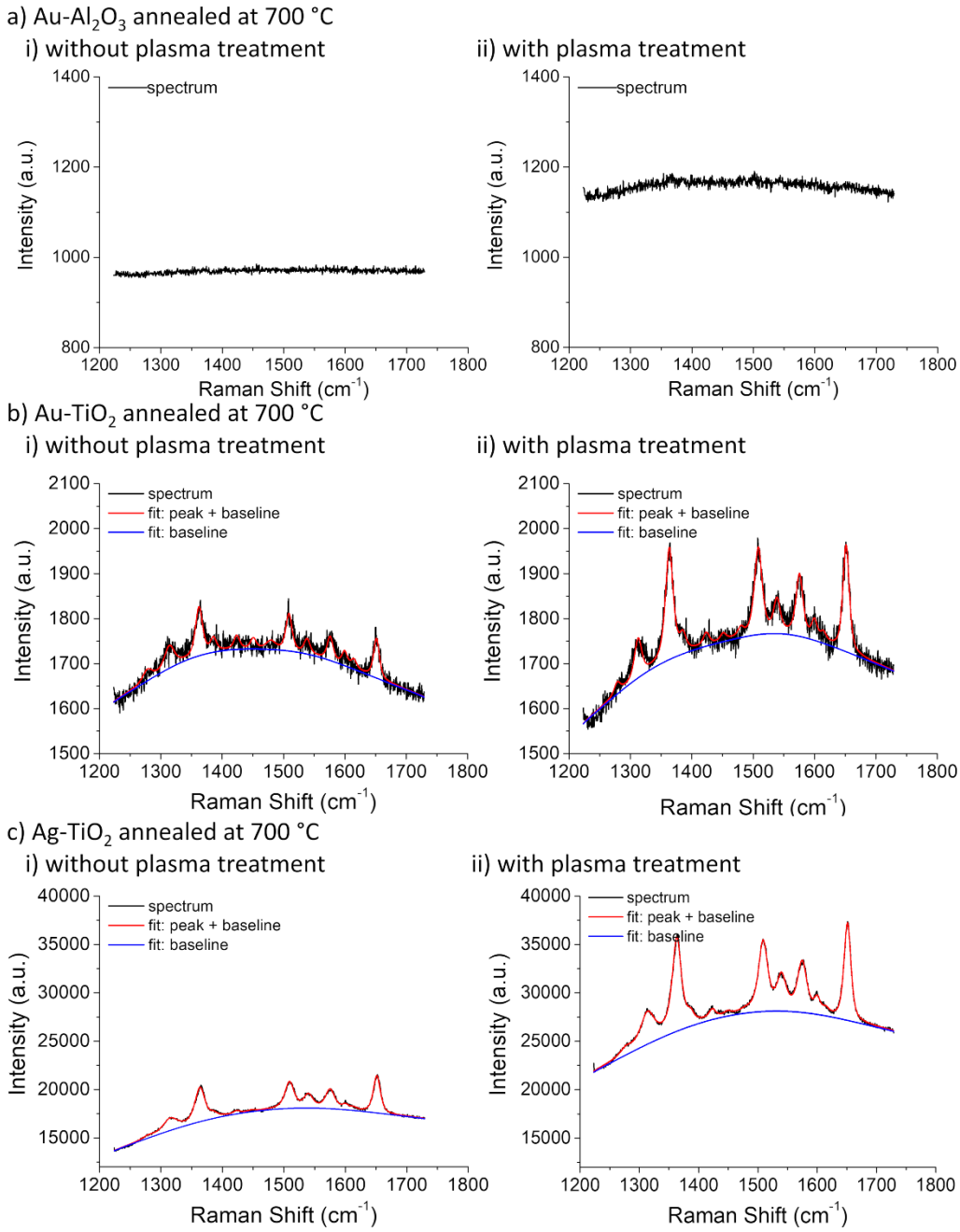

Figure 6 - Observed SERS spectra and the obtained fits for the baseline and total spectrum on a region dominated by R6G modes: (a) Au-Al_2O_3; (b) Au-TiO_2 and (c) Ag-TiO_2, (i) without and (ii) with plasma treatment.

The results for the Raman peak position and relative intensities of the peaks are consistent among the different samples and also to the results reported by Watanabe *et al.* for R6G on Ag [67]. With the obtained intensities, the relative enhancement between the thin films was determined. Table 2

shows the results for the four most intense peaks and the corresponding enhancement factors. Only the results of the four most intense peaks were used, since they provided a more accurate fit than the remaining peaks that don't exhibit a so discernible profile.

Table 2 - Relative Raman intensities of the four most intense R6G peaks, and relative enhancement of each plasmonic thin film.

Sample	Relative Intensity (%)				Relative Enhancement
	Peak 1 (1363 cm^{-1})	Peak 2 (1509 cm^{-1})	Peak 3 (1575 cm^{-1})	Peak 4 (1651 cm^{-1})	
Ag-TiO_2	91	71	51	100	36.6
Ag-TiO_2 w/plasma treatment	95	71	51	100	96.2
Au-TiO_2	100	74	47	80	1.0
Au-TiO_2 w/plasma treatment	100	78	55	96	2.5

These results show that the plasma treatment itself provided a further enhancement of 2.6 times for the Ag-TiO_2 and 2.5 for the Au-TiO_2, in relation to the same thin film without treatment. Yet, by comparing all the tested films, it is clear that the differences between the two systems are much higher, with relative enhancements that can be almost 2 orders of magnitude.

4. Conclusions

In this work, three different systems of nanocomposite plasmonic thin films were deposited by reactive DC magnetron sputtering, changing the dielectric matrix and/or the nanoparticles' noble

metal. These changes allowed to produce the three plasmonic systems: Au-Al_2O_3, Au-TiO_2 and Ag-TiO_2 and to study their differences in terms of chemical, morphological and optical responses.

The content in Au was different for the Al_2O_3 and TiO_2 matrix, about 15 and 13 at.% respectively. The atomic content of Ag in the TiO_2 matrix was higher than Au for the same deposition conditions, about 17 at.%, as silver has a higher sputtering yield.

The structural analysis showed an amorphous Al_2O_3 matrix independently of the post-deposition thermal annealing applied to the Au-Al_2O_3 thin films, while the average size of Au crystalline domains was incremented very smoothly with the increase of annealing temperature. The TiO_2 matrix behaved differently from Al_2O_3, since crystalline domains of anatase, and rutile for the highest temperature (700 ºC), were formed. The Au crystallization in the TiO_2 matrix started also at 300 ºC, however the grain size suffered higher increments when compared to the Al_2O_3 matrix, reaching average values 1 order of magnitude higher. Moreover, an even significant increase was observed in the average grain size of Ag in TiO_2, where the Ag aggregates with sizes in the order of few hundred nm were estimated. Consequently, only the roughness of Ag-TiO_2 films suffered a significant increment due to the migration of Ag cluster to the surface.

Despite the relative low size of Au crystalline domains in Al_2O_3 matrix, these films showed a plasmonic behavior already at 300 ºC, showing narrow LSPR bands and a slight decrease of transmittance minimum with annealing temperature. The Au-TiO_2 films also exhibited a plasmonic behavior at 300 ºC, with a LSPR peak shifted to higher wavelengths since the refractive index of TiO_2 is higher. A broadening of the LSPR band due to the contribution of larger (scattering) nanoparticles over smaller ones was also perceivable. In the thin films with Ag nanoparticles, a well-defined LSPR band was only visible at 500 °C, as this band gives place to a spectrum of almost constant transmittance (broadband absorption) after annealing at 700 °C, associated to the existence of fractal structures on the surface.

Due to their plasmonic behavior, all films were tested as SERS platforms. However, in order to select the best candidates for detection of *e.g.* microorganisms such as *C. albicans* it was pertinent to evaluate if contact with the surface of the films affect cell growth or viability during time. The results suggested no influence in growth behavior of the yeast cells as well as in viability, showing that is possible to use these thin films in biosensing approaches with living microorganisms.

As such, the performed SERS experiments showed that the presence of the Au-TiO_2 and Ag-TiO_2 thin films allowed the observation of R6G Raman scattering, with enhancements of 10^{10} and 10^{11}, respectively, while in Au-Al_2O_3 films, this was not possible. The application of the plasma treatment provided a further enhancement of Raman signals, and the use of Ag nanoparticles instead of Au into a TiO_2 matrix provides a relative enhancement factor close to 10^2.

Acknowledgements

This work was supported by the Portuguese Foundation for Science and Technology (FCT) in the framework of the Strategic Funding UID/FIS/04650/2019 and UID/BIA/04050/2019; and by the projects NANOSENSING POCI-01-0145-FEDER-016902, with FCT reference PTDC/FIS-NAN/1154/2014; and project NANO4BIO POCI-01-0145-FEDER-032299, with FCT reference PTDC/FIS-MAC/32299/2017. Diogo Costa and Marco S. Rodrigues acknowledge FCT for theirs PhD Scholarships, SFRH/BD/136279/2018 and SFRH/BD/118684/2016. Joel Borges acknowledge FCT for his Researcher Contract from project NANO4BIO, CTTI-149/18-CF(1). João Oliveira acknowledges his grant with reference CFUM-BI-04/2018-UID/FIS/04650/2013. The authors also acknowledge Nuno P. Barradas (C2TN, Universidade de Lisboa) and Eduardo Alves (IPFN, Universidade de Lisboa) for the RBS measurements and analysis and Mihai Apreutesei (MATEIS Laboratory-INSA de Lyon) for the XRD analysis with *in situ* thermal annealing.

References

[1] L.M. Liz-Marzán, Tailoring Surface Plasmons through the Morphology and Assembly of Metal Nanoparticles, Langmuir. 22 (2006) 32–41.

[2] S. Eustis, M. a el-Sayed, Why gold nanoparticles are more precious than pretty gold: noble metal surface plasmon resonance and its enhancement of the radiative and nonradiative properties of nanocrystals of different shapes., Chem. Soc. Rev. 35 (2006) 209–217. doi:10.1039/b514191e.

[3] N.C. Lindquist, P. Nagpal, K.M. McPeak, D.J. Norris, S.H. Oh, Engineering metallic nanostructures for plasmonics and nanophotonics, Reports Prog. Phys. 75 (2012) 036501. doi:10.1088/0034-4885/75/3/036501.

[4] J. Dostálek, J. Ladd, S. Jiang, J. Homola, SPR Biosensors for Detection of Biological and Chemical Analytes, in: J. Homola (Ed.), Surf. Plasmon Reson. Based Sensors, Springer Berlin Heidelberg, Berlin, Heidelberg, 2006: pp. 177–190. doi:10.1007/5346_019.

[5] S.S. Yee, J. Homola, S.S. Yee, G. Gauglitz, Surface plasmon resonance sensors: review, Sensors Actuators B. 54 (1999) 3–15. doi:10.1016/S0925-4005(98)00321-9.

[6] A. Paliwal, A. Sharma, M. Tomar, V. Gupta, Optical properties of WO3 thin films using surface plasmon resonance technique, J. Appl. Phys. 115 (2014) 043104. doi:10.1063/1.4862962.

[7] R.L. Rich, D.G. Myszka, Advances in surface plasmon resonance biosensor analysis., Curr. Opin. Biotechnol. 11 (2000) 54–61. doi:10.1016/S0958-1669(99)00054-3.

[8] C.R. Yonzon, E. Jeoung, S. Zou, G.C. Schatz, M. Mrksich, R.P. Van Duyne, A comparative analysis of localized and propagating surface plasmon resonance sensors: The binding of Concanavalin A to a monosaccharide functionalized self-assembled monolayer, J. Am.

Chem. Soc. 126 (2004) 12669–12676. doi:10.1021/ja047118q.

[9] G.A. Lopez, M.C. Estevez, M. Soler, L.M. Lechuga, Recent advances in nanoplasmonic biosensors: Applications and lab-on-a-chip integration, Nanophotonics. 6 (2017) 123–136. doi:10.1515/nanoph-2016-0101.

[10] G. Liang, Z. Zhao, Y. Wei, K. Liu, W. Hou, Y. Duan, Plasma enhanced label-free immunoassay for alpha-fetoprotein based on a U-bend fiber-optic LSPR biosensor, RSC Adv. 5 (2015) 23990–23998. doi:10.1039/C5RA02910D.

[11] M. Estevez, M.A. Otte, B. Sepulveda, L.L.M. Lechuga, Trends and challenges of refractometric nanoplasmonic biosensors: A review, Anal. Chim. Acta. 806 (2014) 55–73. doi:10.1016/j.aca.2013.10.048.

[12] B. Sepúlveda, P.C. Angelomé, L.M. Lechuga, L.M. Liz-Marzán, N. Today, P.C. Angelom, LSPR-based nanobiosensors, Nano Today. 4 (2009) 244–251. doi:10.1016/j.nantod.2009.04.001.

[13] S.J. Zalyubovskiy, M. Bogdanova, A. Deinega, Y. Lozovik, A.D. Pris, K.H. An, W.P. Hall, R.A. Potyrailo, Theoretical limit of localized surface plasmon resonance sensitivity to local refractive index change and its comparison to conventional surface plasmon resonance sensor, J. Opt. Soc. Am. A. 29 (2012) 994. doi:10.1364/JOSAA.29.000994.

[14] D.E. Charles, M. Gara, D. Aherne, D.M. Ledwith, J.M. Kelly, W.J. Blau, M.E. Brennan-Fournet, Scaling of Surface Plasmon Resonances in Triangular Silver Nanoplate Sols for Enhanced Refractive Index Sensing, Plasmonics. 6 (2011) 351–362. doi:10.1007/s11468-011-9211-x.

[15] E. Petryayeva, U.J. Krull, Localized surface plasmon resonance: Nanostructures, bioassays and biosensing-A review, Anal. Chim. Acta. 706 (2011) 8–24.

doi:10.1016/j.aca.2011.08.020.

[16] S.W. Hsu, C. Ngo, A.R. Tao, Tunable and directional plasmonic coupling within semiconductor nanodisk assemblies, Nano Lett. 14 (2014) 2372–2380. doi:10.1021/nl404777h.

[17] J. Ozhikandathil, M. Packirisamy, Simulation and implementation of a morphology-tuned gold nano-islands integrated plasmonic sensor, Sensors (Switzerland). 14 (2014) 10497–10513. doi:10.3390/s140610497.

[18] K.A. Willets, R.P. Van Duyne, Localized Surface Plasmon Resonance Spectroscopy and Sensing, Annu. Rev. Phys. Chem. 58 (2007) 267–297. doi:10.1146/annurev.physchem.58.032806.104607.

[19] M. Piliarik, J. Homola, Surface plasmon resonance (SPR) sensors: approaching their limits?, Opt. Express. 17 (2009) 16505. doi:10.1364/OE.17.016505.

[20] A.J. Haes, R.P. Van Duyne, A unified view of propagating and localized surface plasmon resonance biosensors, Anal. Bioanal. Chem. 379 (2004) 920–930. doi:10.1007/s00216-004-2708-9.

[21] I. Ruach-Nir, T.A. Bendikov, I. Doron-Mor, Z. Barkay, A. Vaskevich, I. Rubinstein, Silica-stabilized gold island films for transmission localized surface plasmon sensing, J. Am. Chem. Soc. 129 (2007) 84–92. doi:10.1021/ja064919f.

[22] G. Cappi, F.M. Spiga, Y. Moncada, A. Ferretti, M. Beyeler, M. Bianchessi, L. Decosterd, T. Buclin, C. Guiducci, Label-Free Detection of Tobramycin in Serum by Transmission-Localized Surface Plasmon Resonance, Anal. Chem. 87 (2015) 5278–5285. doi:10.1021/acs.analchem.5b00389.

[23] S.K. Srivastava, A. Shalabney, I. Khalaila, C. Grüner, B. Rauschenbach, I. Abdulhalim,

SERS Biosensor Using Metallic Nano-Sculptured Thin Films for the Detection of Endocrine Disrupting Compound Biomarker Vitellogenin, Small. 10 (2014) 3579–3587. doi:10.1002/smll.201303218.

[24] C.L. Haynes, A.D. Mcfarland, R.P. Van Duyne, Surface-Enhanced Raman spectroscopy, Anal. Chem. 77 (2005) 339–346.

[25] T.S. Renuga Devi, S. Gayathri, FTIR And FT-Raman spectral analysis of Paclitaxel drugs, Int. J. Pharm. Sci. Rev. Res. 2 (2010) 106–110.

[26] C.W. Freudiger, W. Min, B.G. Saar, S. Lu, G.R. Holtom, C. He, J.C. Tsai, J.X. Kang, X.S. Xie, Label-free biomedical imaging with high sensitivity by stimulated raman scattering microscopy, Science (80-.). 322 (2008) 1857–1861. doi:10.1126/science.1165758.

[27] P.L. Stiles, J.A. Dieringer, N.C. Shah, R.P. Van Duyne, Surface-Enhanced Raman Spectroscopy, Annu. Rev. Anal. Chem. 1 (2008) 601–626. doi:10.1146/annurev.anchem.1.031207.112814.

[28] X. Zhang, M.B.J. Roeffaers, S. Basu, J.R. Daniele, D. Fu, C.W. Freudiger, G.R. Holtom, X.S. Xie, Label-Free Live-Cell Imaging of Nucleic Acids Using Stimulated Raman Scattering Microscopy, ChemPhysChem. 13 (2012) 1054–1059.

[29] J. Grand, M.L. De La Chapelle, J.L. Bijeon, P.M. Adam, A. Vial, P. Royer, Role of localized surface plasmons in surface-enhanced Raman scattering of shape-controlled metallic particles in regular arrays, Phys. Rev. B - Condens. Matter Mater. Phys. 72 (2005) 1–4. doi:10.1103/PhysRevB.72.033407.

[30] L. Billot, M. Lamy de la Chapelle, A.S. Grimault, A. Vial, D. Barchiesi, J.L. Bijeon, P.M. Adam, P. Royer, Surface enhanced Raman scattering on gold nanowire arrays: Evidence of strong multipolar surface plasmon resonance enhancement, Chem. Phys. Lett. 422 (2006)

303–307. doi:10.1016/j.cplett.2006.02.041.

[31] R.M. Hexter, M.G. Albrecht, Metal surface Raman spectroscopy: Theory, Spectrochim. Acta Part A Mol. Spectrosc. 35 (1979) 233–251. doi:10.1016/0584-8539(79)80143-9.

[32] L. Qian, B. Das, Y. Li, Z. Yang, Giant Raman enhancement on nanoporous gold film by conjugating with nanoparticles for single-molecule detection, J. Mater. Chem. 20 (2010) 6891–6895. doi:10.1039/c0jm00884b.

[33] D.G. Leslie, R.E. Kast, J.M. Poulik, R. Rabah, S. Sood, G.W. Auner, M.D. Klein, Identification of pediatric brain neoplasms using raman spectroscopy, Pediatr. Neurosurg. 48 (2012) 109–117. doi:10.1159/000343285.

[34] J.W. Chan, D.S. Taylor, T. Zwerdling, S.M. Lane, K. Ihara, T. Huser, Micro-raman spectroscopy detects individual neoplastic and normal hematopoietic cells, Biophys. J. 90 (2006) 648–656. doi:10.1529/biophysj.105.066761.

[35] R.E. Kast, G.K. Serhatkulu, A. Cao, A.K. Pandya, H. Dai, J.S. Thakur, V.M. Naik, R. Naik, M.D. Klein, G.W. Auner, R. Rabah, Raman spectroscopy can differentiate malignant tumors from normal breast tissue and detect early neoplastic changes in a mouse model, Biopolymers. 89 (2008) 235–241. doi:10.1002/bip.20899.

[36] L. Ashton, K. Lau, C.L. Winder, R. Goodacre, Raman spectroscopy: Lighting up the future of microbial identification, Future Microbiol. 6 (2011) 991–997. doi:10.2217/fmb.11.89.

[37] K. Tintelnot, G. Haase, M. Seibold, F. Bergmann, M. Staemmler, T. Franz, D. Naumann, Evaluation of phenotypic markers for selection and identification of Candida dubliniensis, J. Clin. Microbiol. 38 (2000) 1599–1608.

[38] É.M. Timmins, S.A. Howell, B.K. Alsberg, W.C. Noble, R. Goodacre, Rapid differentiation of closely related Candida species and strains by pyrolysis-mass spectrometry and Fourier

transform-infrared spectroscopy, J. Clin. Microbiol. 36 (1998) 367–374.

[39] E.H. Ibrahim, G. Sherman, S. Ward, V.J. Fraser, M.H. Kollef, The influence of inadequate antimicrobial treatment of bloodstream infections on patient outcomes in the ICU setting, Chest. 118 (2000) 146–155. doi:10.1378/chest.118.1.146.

[40] N.S. Chouthai, A.A. Shah, H. Salimnia, O. Palyvoda, S. Devpura, M. Klein, B. Asmar, Use of Raman spectroscopy to decrease time for identifying the species of Candida growth in cultures, Avicenna J. Med. Biotechnol. 7 (2015) 45–48.

[41] M.S. Ibelings, K. Maquelin, H.P. Endtz, H.A. Bruining, G.J. Puppels, Rapid identification of Candida spp. in peritonitis patients by Raman spectroscopy, Clin. Microbiol. Infect. 11 (2005) 353–358. doi:10.1111/J.1469-0691.2005.01103.X.

[42] K. Jia, J.L. Bijeon, P.M. Adam, R.E. Ionescu, Large Scale Fabrication of Gold Nano-Structured Substrates Via High Temperature Annealing and Their Direct Use for the LSPR Detection of Atrazine, Plasmonics. 8 (2013) 143–151. doi:10.1007/s11468-012-9444-3.

[43] J. Zhao, X. Zhang, C.R. Yonzon, A.J. Haes, R.P. Van Duyne, Localized surface plasmon resonance biosensors, Nanomedicine. 1 (2006) 219–228. doi:10.2217/17435889.1.2.219.

[44] J. Borges, D. Costa, E. Antunes, C. Lopes, M.S. Rodrigues, M. Apreutesei, E. Alves, N.P. Barradas, P. Pedrosa, C. Moura, L. Cunha, T. Polcar, F. Vaz, P. Sampaio, Biological behaviour of thin films consisting of Au nanoparticles dispersed in a TiO_2 dielectric matrix, Vacuum. 122 (2015). doi:10.1016/j.vacuum.2015.03.036.

[45] M. Torrell, M. I., A. Cavaleiro, F. Vaz, Nanocomposite Thin Films Resulting from Au Nanoclusters Dispersed in Titanium Oxide Dielectric Matrixes: the Surface Plasmon Resonance Effect, in: Adv. Nanocomposite Technol., 2011: pp. 89–114. doi:10.5772/18622.

[46] J. Borges, M. Buljan, J. Sancho-Parramon, I. Bogdanovic-Radovic, Z. Siketic, T. Scherer, C.

Kübel, S. Bernstorff, A. Cavaleiro, F. Vaz, A.G. Rolo, Evolution of the surface plasmon resonance of Au:TiO2 nanocomposite thin films with annealing temperature, J. Nanoparticle Res. 16 (2014) 2790. doi:10.1007/s11051-014-2790-7.

[47] J. Borges, M.S. Rodrigues, C. Lopes, D. Costa, F.M. Couto, T. Kubart, B. Martins, N. Duarte, J.P. Dias, A. Cavaleiro, T. Polcar, F. Macedo, F. Vaz, Thin films composed of Ag nanoclusters dispersed in TiO2: Influence of composition and thermal annealing on the microstructure and physical responses, Appl. Surf. Sci. 358 (2015) 595–604. doi:10.1016/j.apsusc.2015.08.148.

[48] R.P. Domingues, M.S. Rodrigues, M. Proença, D. Costa, E. Alves, N.P. Barradas, F.J. Oliveira, R.F. Silva, J. Borges, F. Vaz, Thin films composed of Au nanoparticles embedded in AlN: Influence of metal concentration and thermal annealing on the LSPR band, Vacuum. 157 (2018) 414–421. doi:https://doi.org/10.1016/j.vacuum.2018.09.013.

[49] M. Proença, J. Borges, M.S. Rodrigues, R.P. Domingues, J.P. Dias, J. Trigueiro, N. Bundaleski, O.M.N.D. Teodoro, F. Vaz, Development of Au/CuO nanoplasmonic thin films for sensing applications, Surf. Coatings Technol. 343 (2018) 178–185. doi:10.1016/j.surfcoat.2017.08.033.

[50] M.S. Rodrigues, D. Costa, R.P. Domingues, M. Apreutesei, P. Pedrosa, N. Martin, V.M. Correlo, R.L. Reis, E. Alves, N.P. Barradas, P. Sampaio, J. Borges, F. Vaz, Optimization of nanocomposite Au/TiO 2 thin films towards LSPR optical-sensing, Appl. Surf. Sci. 438 (2018) 74–83. doi:10.1016/j.apsusc.2017.09.162.

[51] N.P. Barradas, C. Jeynes, R.P. Webb, U. Kreissig, R. Grötzschel, Unambiguous automatic evaluation of multiple Ion Beam Analysis data with Simulated Annealing, Nucl. Instruments Methods Phys. Res. Sect. B Beam Interact. with Mater. Atoms. 149 (1999) 233–237. doi:10.1016/S0168-583X(98)00731-9.

[52] N.P. Barradas, M.A. Reis, Accurate calculation of pileup effects in PIXE spectra from first principles, X-Ray Spectrom. 35 (2006) 232–237. doi:10.1002/xrs.903.

[53] N.P. Barradas, C. Pascual-Izarra, Double scattering in RBS analysis of PtSi thin films on Si, Nucl. Instruments Methods Phys. Res. Sect. B Beam Interact. with Mater. Atoms. 228 (2005) 378–382. doi:https://doi.org/10.1016/j.nimb.2004.10.074.

[54] A. Rühm, B.P. Toperverg, H. Dosch, Supermatrix approach to polarized neutron reflectivity from arbitrary spin structures, Phys. Rev. B. 60 (1999) 16073–16077. doi:10.1103/PhysRevB.60.16073.

[55] J. Borges, M.S. Rodrigues, T. Kubart, S. Kumar, K. Leifer, M. Evaristo, A. Cavaleiro, M. Apreutesei, R.M.S. Pereira, M.I. Vasilevskiy, T. Polcar, F. Vaz, Thin films composed of gold nanoparticles dispersed in a dielectric matrix: The influence of the host matrix on the optical and mechanical responses, Thin Solid Films. 596 (2015). doi:10.1016/j.tsf.2015.08.058.

[56] J.F. Pierson, D. Wiederkehr, A. Billard, Reactive magnetron sputtering of copper, silver, and gold, Thin Solid Films. 478 (2005) 196–205. doi:10.1016/j.tsf.2004.10.043.

[57] J. Borges, C.G. Ferreira, J.P.C. Fernandes, M.S. Rodrigues, M. Proença, M. Apreutesei, E. Alves, N.P. Barradas, C. Moura, F. Vaz, Thin films of Ag-Au nanoparticles dispersed in TiO2: Influence of composition and microstructure on the LSPR and SERS responses, J. Phys. D. Appl. Phys. 51 (2018) 205102. doi:10.1088/1361-6463/aabc49.

[58] M.S. Rodrigues, J. Borges, C. Gabor, D. Munteanu, M. Apreutesei, P. Steyer, C. Lopes, P. Pedrosa, E. Alves, N.P. Barradas, L. Cunha, D. Martínez-Martínez, F. Vaz, Functional behaviour of TiO2 films doped with noble metals, Surf. Eng. 32 (2016) 554–561. doi:10.1179/1743294415Y.0000000085.

[59] J. Borges, T. Kubart, S. Kumar, K. Leifer, M.S. Rodrigues, N. Duarte, B. Martins, J.P. Dias,

A. Cavaleiro, F. Vaz, Microstructural evolution of Au/TiO2 nanocomposite films: The influence of Au concentration and thermal annealing, Thin Solid Films. 580 (2015) 77–88. doi:10.1016/j.tsf.2015.03.024.

[60] J. Borges, M.S. Rodrigues, C. Lopes, D. Costa, A. Ferreira, R.M.S. Pereira, M.F. Costa, M.I. Vasilevskiy, F. Vaz, Ag fractals formed on top of a porous TiO_2 thin film, Phys. Status Solidi - Rapid Res. Lett. 10 (2016) 530–534. doi:10.1002/pssr.201600131.

[61] A.I. Barbosa, J. Borges, D.I. Meira, D. Costa, M.S. Rodrigues, R. Rebelo, V.M. Correlo, F. Vaz, R.L. Reis, Development of label-free plasmonic Au-TiO2 thin film immunosensor devices, Mater. Sci. Eng. C. 100 (2019) 424–432. doi:10.1016/J.MSEC.2019.03.029.

[62] S. koneti, J. Borges, L. Roiban, M.S. Rodrigues, N. Martin, T. Epicier, F. Vaz, P. Steyer, Electron Tomography of Plasmonic Au Nanoparticles Dispersed in a TiO 2 Dielectric Matrix, ACS Appl. Mater. Interfaces. 10 (2018) acsami.8b16436. doi:10.1021/acsami.8b16436.

[63] E.P. Ivanova, V.K. Truong, J.Y. Wang, C.C. Bemdt, R.T. Jones, I.I. Yusuf, I. Peake, H.W. Schmidt, C. Fluke, D. Barnes, R.J. Crawford, Impact of nanoscale roughness of titanium thin film surfaces on bacterial Retention, Langmuir. 26 (2010) 1973–1982. doi:10.1021/la902623c.

[64] J. Borges, R.M.S. Pereira, M.S. Rodrigues, T. Kubart, S. Kumar, K. Leifer, A. Cavaleiro, T. Polcar, M.I. Vasilevskiy, F. Vaz, Broadband Optical Absorption Caused by the Plasmonic Response of Coalesced Au Nanoparticles Embedded in a TiO2 Matrix, J. Phys. Chem. C. 120 (2016) 16931–16945. doi:10.1021/acs.jpcc.6b03684.

[65] E.C. Le Ru, E. Blackie, M. Meyer, P.G. Etchegoint, Surface enhanced raman scattering enhancement factors: A comprehensive study, J. Phys. Chem. C. 111 (2007) 13794–13803. doi:10.1021/jp0687908.

[66] M. Moores, K. Gracie, J. Carson, K. Faulds, D. Graham, M. Girolami, Bayesian modelling and quantification of Raman spectroscopy, (2016).

[67] H. Watanabe, N. Hayazawa, Y. Inouye, S. Kawata, DFT vibrational calculations of Rhodamine 6G adsorbed on silver: Analysis of tip-enhanced Raman spectroscopy, J. Phys. Chem. B. 109 (2005) 5012–5020. doi:10.1021/jp045771u.

[68] S. Nie, S.R. Emory, Probing single molecules and single nanoparticles by surface-enhanced Raman scattering, Science (80-.). 275 (1997) 1102–1106. doi:10.1126/science.275.5303.1102.

[69] P. Hildebrandt, M. Stockhurger, Surface-Enhanced Resonance Raman Spectroscopy of Rhodamine 6G adsorbed on colloidal silver, J. Phys. Chem. 88 (1984) 5935–5944. doi:10.1021/j150668a038.